Accepted for publication in Building & Environment, August 2014

CFD simulation and validation of urban microclimate: A case study for Bergpolder Zuid, Rotterdam

Y. Toparlar*[1,2)], B. Blocken[1,3)], P. Vos[2)], G.J.F. van Heijst[4)], W.D. Janssen[1)], T. van Hooff[1)], H. Montazeri[1)], H.J.P. Timmermans[5)]

1) Building Physics and Services, Department of the Built Environment, Eindhoven University of Technology, Eindhoven, the Netherlands
2) Environmental Modeling, Flemish Institute for Technological Research, Mol, Belgium
3) Building Physics Section, Department of Civil Engineering, Leuven University, Heverlee, Belgium
4) Fluid Dynamics Laboratory, Department of Applied Physics, Eindhoven University of Technology, Eindhoven, the Netherlands
5) Urban Science and Systems, Department of the Built Environment, Eindhoven University of Technology, Eindhoven, the Netherlands
**) Corresponding author: Yasin Toparlar, Building Physics and Services, Eindhoven University of Technology, P.O. box 513, 5600 MB, Eindhoven, the Netherlands. Tel. +31 (0)40 247 8444, Fax: +31 (0)40 243 8595, e-mail: y.toparlar@tue.nl*

Abstract

Considering climate change and the rapid trend towards urbanization, the analysis of urban microclimate is gaining importance. The Urban Heat Island (UHI) effect and summer-time heat waves can significantly affect urban microclimate with negative consequences for human mortality and morbidity and building energy demand. So far, most studies on urban microclimate employed observational approaches with field measurements. However, in order to provide more information towards the design of climate adaptive urban areas, deterministic analyses are required. In this study, Computational Fluid Dynamics (CFD) simulations are performed to predict urban temperatures in the Bergpolder Zuid region in Rotterdam, which is planned to be renovated to increase its climate resilience. 3D unsteady Reynolds-averaged Navier-Stokes (URANS) simulations with the realizable k-ε turbulence model are performed on a high-resolution computational grid. The simulations include wind flow and heat transfer by conduction, convection and radiation. The resulting surface temperatures are validated using experimental data from high-resolution thermal infrared satellite imagery performed during the heat wave of July 2006. The results show that the CFD simulations are able to predict urban surface temperatures with an average deviation of 7.9% from the experimental data. It is concluded that CFD has the potential of accurately predicting urban microclimate. Results from CFD simulations can therefore be used to identify problem areas and to evaluate the effect of climate adaptation measures in these areas such as urban greening and evaporative cooling.

Keywords: Urban environment; Climate adaptation; Building aerodynamics; Heat stress and thermal comfort; Built environment; Urban physics.

1. Introduction

The adverse effect of high temperatures on human morbidity and mortality and energy use in buildings has been investigated in various studies about climate change [1–3] and heat waves [4–6]. Because of the Urban Heat Island (UHI) effect, the negative consequences of high temperatures are even more severe inside urban areas [7–11]. The UHI refers to the fact that temperatures in urban areas are generally higher than the surrounding rural areas, because urban areas retain and release more heat to their local environment. In view of the rapid trend towards urbanization [12,13], the design of sustainable and comfortable urban spaces and buildings becomes increasingly important [14]. In this perspective, the study of urban microclimate is a key element during the design stages of urban settlements, whether it concerns a new project or a redevelopment project [15,16].

Although there are several subtopics which can be a part of urban microclimate research (e.g. wind flow, water balance, energy exchange), the urban temperature field and consequently the UHI effect constitute some of the most common subjects covered [17]. According to the review paper by Mirzaei and Haghighat [18], techniques to study the urban heat island effect can be divided into two groups. One is termed “observational approaches” which can be

field measurements, thermal remote sensing or small-scale modeling (models built for wind-tunnel tests or for measurements in the outdoor environment). The other group is called “simulation approaches” which can be either energy balance models or numerical studies using Computational Fluid Dynamics (CFD). The main advantage of simulation studies compared to observational studies is the possibility to perform comparative analyses based on different scenarios. Moreover, as opposed to observational studies, simulations can provide results for any relevant variable in the whole computational domain. On the other hand, the main drawback of simulation approaches is the necessity to apply several simplifications, as the physics underlying the urban microclimate is very complex. Therefore, careful validation of the simulations is very important.

Among the simulation approaches, the energy balance model [19], which is based on energy conservation for a control volume, is extensively used in the UHI research. A range of studies investigated the parameterization [20–23] and the implementation of this model for various urban regions [24–27]. The main weakness of this model is the absence of the velocity field [18] which implies the decoupling of temperature and wind flow. Lower wind velocities inside street canyons and courtyards cause a decrease in heat transferred out of the local environment, which substantially affects the UHI effect [28]. Therefore, the absence of the velocity field is a serious limitation in urban microclimate research conducted with energy balance models. In that sense, CFD can be a useful tool for coupling temperature and velocity fields, but it requires high-resolution modeling of urban areas, the knowledge of relevant boundary conditions and sufficient computational resources for the simulations [29,30]. As the use of CFD in urban physics continues to gain popularity, several guidelines [31–36] have been published to improve the quality of the simulations and to limit numerical and physical modeling errors.

CFD is widely used in urban physics [16,30,37,38]. Applications include pedestrian-level wind conditions [37,39–42], pollutant dispersion [43–47], wind-driven rain [48,49], natural ventilation [50–53] and thermal environment in urban areas [54–77]. An overview of 24 previous CFD studies on the thermal environment in urban areas is provided in Table 1, distinguishing between mesoscale and microscale studies. In a mesoscale CFD simulation, the analysis of urban climate spans a larger area than microclimate (scale of a microclimate study is often less than 10 km). Because of the larger scale in mesoscale studies, the buildings are generally not modeled explicitly, which means neglecting (or averaging) several contributing factors like wind flow inside street canyons and building shapes. This simplification has a direct influence on radiative and convective heat transfer and thus on the microscale thermal environment. For every study, Table 1 indicates which UHI causes were considered. Indeed, in order to simulate urban microclimate accurately, several physical phenomena should be considered, which can be expressed as UHI causes. Oke [19,28] identified the following possible UHI causes (Figure 1) :

1. Amplified short-wave radiation gain;
2. Amplified long-wave radiation gain from the sky;
3. Decreased long-wave radiation loss;
4. Anthropogenic heat sources inside urban areas;
5. Increased heat storage;
6. Less evapotranspiration;
7. Decreased turbulent heat transport.

All these causes negatively affect the urban thermal environment. Amplified short-wave radiation gain refers to the fact that more solar radiation is absorbed due to multiple reflections in the urban environment. Amplified long-wave radiation gain from the sky originates from the air pollution over urban areas, which causes an additional radiation load. Decreased long-wave radiation loss is caused by buildings acting as obstructions and keeping part of the long-wave emission within street canyons. Anthropogenic heat sources are those resulting from human activity (cars, industry etc.). Increased heat storage in the urban environment, caused by the use of construction materials (pavement, asphalt, some building materials, etc.), is another important factor affecting the urban thermal environment. Less evapotranspiration is associated with the lack of moisture availability inside urban areas (less vegetation, less water sources etc.). Decreased turbulent heat transport refers to lower wind velocity in courtyards and street canyons and to the resulting decreased convective heat transfer and urban ventilation.

Table 1 also indicates the scales of the studies, which type of buildings or urban configurations were considered, whether the simulations were steady or unsteady and whether a validation study was conducted. CFD can potentially provide accurate information on urban wind flow and heat transfer. If it would be shown that accurate results can be obtained for complex case studies, such simulations could be used to analyze urban thermal environment and to evaluate the effectiveness of adaptation measures in real urban areas. To judge whether a proposed CFD approach is capable of performing a complex analysis of urban microclimate, the study should be conducted at the microscale with a real (applied) urban case with buildings. To model the urban thermal environment correctly, the simulations

should consider most of the "possible causes" and should follow an unsteady approach. Finally, to increase the reliability of a CFD approach, validation of the simulation results is required.

According to Table 1, the number of publications about the CFD analysis of urban thermal environment has increased over the years. Considering the scales investigated, only a few of the mentioned studies are conducted at the mesoscale [54,58]. Studies at the microscale with 2D computational domains [56,57,69,70] are common but mostly conducted to investigate several fundamental parameters about the flow field or the temperature field. Among the remaining studies (microscale 3D), only a few of them have considered an applied urban case and supported the results with a validation study [59,60,63,73,76]. The study by Yang et al. [76] contains the most complex simulation setup when the number of physical models is considered. Although that study has been performed at a real urban area (Guangzhou), the main investigation was the thermal behavior of different ground surfaces. In the computational domain of Yang et al. [76], only a few buildings were present and the area of interest was not a dense urban environment. Therefore it is necessary to conduct a study which is as comprehensive as the one by Yang et al. [76], but focused on a real and complex urban setting. This is the focus of the present paper.

This study is a 3D microscale study in which the buildings are modeled explicitly and based on a real urban area (3D applied urban configuration). Among the possible UHI causes suggested by Oke [19,28], only the effect of anthropogenic heat sources is neglected. The simulations consider wind flow and heat transfer (conduction, convection, radiation). They are conducted using the 3D unsteady Reynolds Averaged Navier-Stokes (URANS) equations with the realizable k-ε turbulence model [78] on a high-resolution and high-quality computational grid. Validation is conducted for the surface temperatures during the 2006 heat wave, which were measured using satellite imagery and reported by Klok et al. [79]. After the validation study, the urban microclimate of Bergpolder Zuid is analyzed and the effect of wind velocity on the temperature field is shown.

In Section 2, the problem statement and the urban area are briefly described. In Section 3, the urban geometry, the computational domain, the grid and other computational settings and parameters are outlined. Section 4 presents the CFD validation for the surface temperatures. In Section 5, air temperatures inside the urban area are evaluated for an entire day. Finally, the paper concludes with Section 6 (discussion) and Section 7 (conclusion).

2. Problem statement and urban area

2.1 Problem statement

Several research organizations and consortia have initiated programs and projects on climate change adaptation in cities as the Intergovernmental Panel on Climate Change (IPCC) has continued to express the importance of adaptation measures [80]. Climate Proof Cities (CPC) is a consortium of universities, research institutes, policy makers and city officials that aims at performing basic and applied research on climate adaptation of urban areas [81]. It includes case studies for several locations in the Netherlands. One of these locations is the Bergpolder Zuid region in Rotterdam, located in the Noord district of the city (Figure 2a). The region is planned to be renovated and the CPC consortium evaluates several climate change adaptation measures for potential implementation in this region. Because of the densely built environment of Rotterdam, basic symptoms of the UHI effect are present, as demonstrated in earlier studies [79,82]. According to Klok et al. [79], average surface temperatures inside Rotterdam can reach up to 45°C during heat waves, which is clearly undesirable. Moreover, according to the same study, the maximum average surface temperature differences between the warmest and the coolest districts of Rotterdam were 12°C during day and 9°C during nighttime.

As mentioned earlier, the numerical analysis of urban microclimate is important during the design stages of an urban redevelopment project. The aim of the present study is to analyze the accuracy and suitability of CFD for this type of application and to gain more insight in the temperature distribution inside the Bergpolder Zuid region under the meteorological conditions of a heat wave.

2.2 Urban area and surroundings

The Bergpolder Zuid region is composed of both residential and office buildings with several narrow streets and surrounded by large avenues (Figure 2). Here, the classification of streets is made with respect to the aspect ratio between the street width and the adjacent building height. In general, most of the streets are narrow with an aspect ratio between 1:1 and 2:1.

The main color of the building walls is red and the rooftops are commonly grey or dark grey. Street materials generally have lighter colors (light grey) compared to the building materials. The vegetation levels of the region are fairly low as trees and green fields are mostly located in a few small courtyards. The only urban water source is the

canal located in the north of the region and there are no additional water facilities within the neighborhood, meaning the region has low evapotranspiration levels, which is typical of dense metropolitan cities.

In order to create an accurate geometrical model of the region, official drawings and documents were acquired from the Municipality of Rotterdam and from the database of AHN[1]. According to the database, the average height of buildings is 12.6 m with the lowest building having a height of 2.8 m and the highest building of 51.0 m.
Considering the surroundings of the Bergpolder Zuid region, to the south lays the central district of Rotterdam and to the north, mainly green fields are found until the city of Delft (located in the northwest). Based on the updated Davenport roughness classification [83], the aerodynamic roughness length (z_0) of the surroundings, which is necessary as input for the CFD simulations, is determined as shown in Figure 3. The z_0 value is determined as a spatial average of the z_0 values of the different patches of roughness (land use) of the terrain within a 10 km radius upstream of the urban area. A similar methodology was followed in previous CFD studies investigating urban wind flow [36, 42].

3. CFD simulations: computational settings and parameters

3.1 Computational domain and grid

The computational domain used in this study is hexagonal and contains a circular subdomain that includes the buildings (Figure 3 and Figure 4). The edges of the hexagon are 1200 m, yielding an area with a maximum distance of 2400 m. The hexagonal domain surrounds the circular subdomain, which has a diameter of 1200 m (Figure 4). The buildings inside the circular subdomain are modeled explicitly (i.e. with their main shape and dimensions) and divided into three categories: (1) buildings in Bergpolder Zuid; (2) buildings in the rest of the Bergpolder region; and (3) the surrounding buildings. The buildings inside Bergpolder Zuid are modeled with high resolution, down to details of 0.5 m. Buildings in the rest of the Bergpolder region are modeled more coarsely with details of 1.0 m. As suggested by the CFD best practice guidelines [33,35], at least one additional street block around the area of interest (in this case, Bergpolder Zuid) should also be modeled. These surrounding buildings should be placed only to act as obstacles for the approaching wind flow. They are modeled coarsely with details of 4.0 m to 8.0 m. Remaining elements like trees, street poles, cars are not modeled, and this issue is referred to in the discussion section.

Outside the circular subdomain, buildings and other urban forms (such as streets, parks, roads) are not modeled explicitly but rather they are represented by using appropriate roughness parameters in the wall functions. The equivalent sand-grain roughness height (k_S) and roughness constant (C_S) are determined considering their relationship with the aerodynamic roughness length [34] at the bottom of the domain. The height of the domain is 400 m (see Figure 4). The maximum blockage ratio is 1.8%, which is less than the recommended value of 3% [33,35].

Generation of the computational grid is based on the same methodology as introduced by van Hooff & Blocken [36], which starts by meshing the ground plane followed by the extrusion of the ground surface grid along a third axis for obtaining the three-dimensional grid. The grid is finer in the area of interest (Bergpolder Zuid) but as the distance from the target area increases, the grid becomes coarser. Special attention is given to the guidelines of Franke et al. [33] and Tominaga et al. [35] by using at least ten cells on the building edges and by keeping the grid stretching ratio below 1.3. This results in a grid with 6,610,456 hexahedral cells (see Figure 5).

3.2 Boundary conditions

A flow boundary condition either as velocity inlet or pressure outlet is imposed on each outer face of the hexagonal domain, depending on the wind direction simulated. In every simulation, three of these boundaries are specified as velocity inlets and the remaining three as outlets. Meteorological data used in this study are obtained from the Royal Dutch Meteorological Institute (KNMI) by the Rotterdam weather station, which is located near Rotterdam airport approximately 4 km northwest of Bergpolder Zuid (Figure 3).

At the inlets, a logarithmic mean wind speed profile (U) (m/s) (Eq. 1) is imposed with z_0 = 0.5 m or z_0 = 1.0 m, depending on the wind direction (Figure 3). The reference wind speed depends on the hourly meteorological data and varies between 1 m/s and 6 m/s at 10 m height (U_{10}).

$$\boldsymbol{U(z) = \frac{u^*}{\kappa} \ln\left(\frac{z+z_0}{z_0}\right)} \quad (1)$$

[1] AHN: Actueel Hoogtebestand Nederland (Updated Height data of the Netherlands) http://www.ahn.nl/

Turbulent kinetic energy (k) (m^2/s^2) and turbulence dissipation rate (ε) (m^2/s^3) are given by [84]:

$$\boldsymbol{k} = \frac{\boldsymbol{u^{*2}}}{\sqrt{\boldsymbol{C_\mu}}} \tag{2}$$

$$\boldsymbol{\varepsilon(z)} = \frac{\boldsymbol{u^{*3}}}{\boldsymbol{\kappa(z+z_0)}} \tag{3}$$

In these equations, κ is the von Karman constant (= 0.41), u^* (m/s) is the atmospheric boundary layer friction velocity, C_μ is a constant (= 0.09), z_0 (m) is the aerodynamic roughness length and z (m) is the height coordinate. At the inlet, a spatially constant air temperature is imposed and its value and time dependency is given by the hourly weather data.

At the walls, the standard wall functions [85] are used in combination with the sand-grain based roughness modification [86] and the parameters k_S (roughness height) and C_S (roughness constant) are determined from their appropriate relationship with z_0. The relationship between these parameters depends on the CFD software used. In this study, the commercial CFD software ANSYS Fluent 12 is used and for this software, the relationship is given by Blocken et al. [34]:

$$\boldsymbol{k_S} = \frac{\boldsymbol{9.793 z_0}}{\boldsymbol{C_S}} \tag{4}$$

Appropriate and consistent roughness parameters should be specified to obtain a horizontally homogeneous atmospheric boundary layer in the upstream part of the computational domain [34,84]. Horizontal homogeneity implies the absence of stream-wise gradients in the vertical profiles of the mean wind velocity and turbulence quantities. The ANSYS Fluent software does not allow any k_S value higher than z_p, which is the distance between the center point of the wall-adjacent cell to the wall. Therefore, Cs values are increased instead.

In combination with Eq. 4, this yields: for the hexagonal domain, k_S = 1.39 m and C_S = 3.5 (for z_0 = 0.5 m) and k_S = 1.39 m and C_S = 7 (for z_0 = 1.0 m). Inside the circular domain, the ground plane is modeled as z_0 = 0 m.

Apart from the standard wall functions, the near-wall region could be resolved with low-Re number modeling, which would mean placing control volumes in every part of the often very thin boundary layer near the wall surface (namely thin viscous sub-layer, the buffer layer and the logarithmic layer). However, this modeling approach would require an excessively high grid resolution, which would very strongly increase the computational load [87]. Although it is stated in various studies that the wall functions might not perform well for the calculation of convective heat transfer [88], this method is still widely used to calculate convective heat transfer implicitly at the surface [87].

The ground plane of the computational domain is modeled implicitly as a 10 m thick earth layer with a constant temperature of 10°C at 10 m below ground. The internal air inside the buildings is assumed to be at 24°C and building walls are composed of brick materials with 0.4 m thickness. Material specifications of earth and brick (for building walls and roofs) as used in this study can be found in Table 2. The absorptivity and emissivity of the materials provided in Table 2 have the same values for both shortwave and longwave radiation. Considering the fact that the windows are not modelled in the simulations, no transmissivity is considered for the building surfaces. Therefore the shortwave reflectivity or albedo value is (1 – absorptivity). Here, it should be noted that the material specifications of earth resemble a generic earth material for density, specific heat and thermal conductivity but for reflective properties like solar absorptivity and emissivity, specifications are based on light colored concrete. The reason for this choice is to resemble the top of the 10 m thick ground plane as light colored concrete, which is the dominant road pavement material in Bergpolder Zuid.

The top of the computational domain is modeled as a free-slip wall, which assumes zero normal gradients for all the variables. At the outlets, zero static pressure is imposed.

Total solar radiation is also acquired from the hourly weather data (to be shown in section 4). In this study, the effect of anthropogenic heat sources is omitted. As for evapotranspiration in day time, during morning (6:00-11:00 h) and afternoon (15:00-18:00 h) a constant sink value of 80 W/m^2 is implemented and during noon time, the sink value is 130 W/m^2. The sink value of evapotranspiration is only applied for the ground plane and not on building surfaces. This assumption is in accordance with the observations from previous measurement studies [20,27,89] considering heat fluxes inside dense urban areas.

3.3 Other computational parameters

The 3D URANS equations are solved with the realizable k-ε turbulence model [78] for closure. For the radiation equations, the P-1 radiation model is used [90] and the Boussinesq approximation is used for buoyancy. For the ground and building walls, a one-directional conduction equation, which calculates heat transfer between two sides of the walls, is applied. Ideally, a three-dimensional approach can be followed to consider heat transfer within the planar directions of the walls, which is an issue that will be discussed later in this paper. Parameters such as sun direction vector and the diffuse portion of the total radiation coming to the surface are calculated with the implemented solar calculator of ANSYS Fluent [90]. The solar calculator considers a beam using the position of the sun at any time during a year and applies radiative heat flux on all of the wall type boundaries. The absorption of the radiative heat by the surfaces depends on the absorptivity values shown in Table 2. Heat storage by the solid regions is calculated based on the thermal diffusivity (m^2/s) of the respective materials.

Pressure-velocity coupling is handled with the SIMPLE algorithm and pressure interpolation is second order. Second order discretization schemes are used for all the convection and viscous terms. Second order implicit time integration is used for temporal discretization. Unsteady simulations are performed with 15-minute (900 seconds) time steps, and each time step was calculated with 60 iterations, based on a time-step sensitivity analysis. The scaled residuals at the end of each time step reached the following minimum values: 10^{-4} to 10^{-5} for x, y and z velocity, 10^{-4} for k and ε, 10^{-7} for energy and radiation, 10^{-3} to 10^{-4} for continuity. All simulations are performed considering five consecutive days (120 hours), which corresponds to a total of 480 time steps. With this approach, it is possible to evaluate the diurnal variation of the temperature field.

4. CFD simulations: results and validation

Klok et al. [79] investigated the UHI effect in Rotterdam based on surface temperatures obtained from the thermal images acquired during the July 2006 heat wave by the NOAA-AVHHR[2] satellite. AVHRR has a high temporal resolution (able to monitor diurnal behavior of surface temperatures) and medium spatial resolution of 1.1 km. The satellite imagery data reported by Klok et al. [79] are for 15, 16, 17,18 and 19 July, 2006. Meteorological data for these days are depicted in Figure 6. The wind direction on 15, 16, 17 and 19 July is mainly from north, northeast and east whereas on 18 July some southeast wind was also observed.

The surface temperatures reported by Klok et al. [79] are averaged over each district and do not consider any maximum or minimum values. There is only a single value reported per district. The data of spatially averaged values do not have any additional information about standard deviation and therefore, minimum or maximum surface temperature values cannot be compared in this validation study. Therefore, the comparison between the satellite imagery data and CFD simulation results is only performed for the spatially averaged values.

To extract spatially averaged values from the CFD simulations, several sampling points located on a grid were placed over Bergpolder Zuid. The number of sampling points was based on a sensitivity analysis for a given moment in time. The sensitivity analysis is based on the percentage deviation of average surface temperatures (CFD versus measurements) for 12:10 h on 15 July 2006, when the measured average surface temperature in the Noord district was around 30.5°C. The result of the sensitivity analysis is provided in Figure 7. Following the sensitivity analysis, 90 sampling points are placed on the building roofs and street surfaces of the computational domain of Bergpolder Zuid (see Figure 8). The simulation results of average surface temperatures are the averages over these 90 points.

Although simulations are performed for five complete and consecutive days (120 hours), Klok et al. [79] have reported average surface temperatures for 42 specific times within these five days. At these specific times, the reported average surface temperatures are only momentary, which means meteorological conditions at that moment are likely to be different from hourly averaged meteorological data. Nevertheless, the CFD simulations have been performed with boundary conditions that are updated every hour based on the hourly averaged meteorological data. The CFD simulation results are compared with the experimental data in Figure 9.

In general, a fair to good agreement is observed, especially in terms of diurnal variation. The minimum, average and maximum deviations of surface temperature are 0.27% (19^{th} of July, 18:38 h), 7.9% and 24.2% (16^{th} of July, 8:13 h), respectively. The surface temperature amplitude is smaller in satellite imagery data than in the simulations. Deviations are especially present during the noontime of 18^{th} of July.

Different reasons can be held responsible for the deviations between the CFD simulations and the reported data from the satellite images:

[2] NOAA – AVHRR: US National Oceanic and Atmospheric Administration – Advanced Very High Resolution Radiometer

1. The one-directional wall conduction approach used at the wall boundaries. In reality, some of the heat is transferred in the planar directions of the ground, building walls and roofs (for instance in between warm regions and shaded areas), which increases the thermal inertia of the respective solid zone. However, with the imposed one-directional wall conduction, the effect of planar conduction is omitted and thus, the ground level is more prone to sudden changes in temperature, which might explain the difference in daily surface temperature variance.
2. The effect of relative humidity. In these five days, relative humidity is very unstable. Average daily relative humidity among these five days changes from 49% to 64% and within a single day, e.g. on 18 July, it can decrease from 96% to 32% within only 7 hours. These sudden changes in relative humidity can influence the results as the humidity is not directly considered in the simulations but only indirectly as an evapotranspirational sink.
3. The comparison of momentary experimental data with CFD simulations based on hourly averaged meteorological data. Especially within the days where the hourly variation of wind speed and solar radiation is high, hourly data could not be sufficient to produce accurate results.
4. Uncertainties in the reported satellite imagery data. The satellite imagery data reported by Klok et al. [79] presents a single value for a specific moment and for an entire district. The modeled Bergpolder Zuid region in Rotterdam constitutes only 20% of the complete Noord district. Therefore local conditions in the complete district of Noord might not resemble the conditions inside Bergpolder Zuid region at all times.
5. The thermal stratification of the atmospheric boundary layer (ABL). Considering the wind flow, a neutral ABL is assumed to be present in the surface layer with constant uniform temperature. Especially during times with low wind speed, the actual flow field in the urban environment might deviate from the simulated one because of this assumption.

5. Evaluation of the simulation results

One of the reasons for the UHI effect is the additional heat storage of building materials inside urban areas and its release – mainly during nighttime. In Figure 10, this mechanism is depicted using the CFD simulation results of surface temperature for 16 July 2006. Although at 23:00 (Figure 10d) incoming solar radiation is zero, there is still heat accumulated within the urban environment: According to the meteorological data, air temperature at that time is around 17.0°C but average surface temperatures are much higher (21.8°C). The heat, which is accumulated within the construction materials, is released during the night time, which is apparent in Figure 9. The average surface temperatures continue to decrease, as long as the air temperature is higher. The decrease continues in average surface temperatures continue until the sunrise of the next day.

Another important factor contributing to the UHI effect is the decreased turbulent heat transport inside urban regions. As the wind velocity might drop significantly in the courtyards or in the streets, which are positioned perpendicular to the prevailing wind direction, the ventilative cooling effect of the wind is proportionally reduced. Moreover, in these locations, convected air close to the hot surface cannot leave the local environment, which decreases heat release from surfaces. These effects can be observed by the simulations performed in this study. In Figure 11, contours of wind velocity at 1 meter height and surface temperatures at 10:00 h on 15 July are provided. In the regions with low wind velocity, surface temperatures are noticeably higher. Therefore, the methodology used in this study can be considered as a reliable source to pinpoint critical locations with possibly higher temperatures during warm and sunny days. Further CFD research about urban microclimate can focus on topics to mitigate this negative effect, for instance by better ventilation of the streets or by creating airflow through courtyards.

6. Discussion

The created urban geometry in this research is based on the drawings and data from the municipality of Rotterdam. However, there are elements in reality that are not taken into account in the model. Trees, street poles, cars, balconies, canopies and similar details that might affect the incoming solar radiation are neglected.

Due to the scale of this study and the lack of detailed information, the construction materials of the buildings and at the ground surfaces are considered to have the same properties throughout the domain. In a real urban environment, material use can be different for each building and street and this can locally influence the temperature field.

The vertical inlet profiles of mean velocity (U), turbulent kinetic energy (k) and turbulence dissipation rate (ε) are taken from Richards & Hoxey [84]. These profiles were derived as analytical solutions of the standard k-ε

turbulence model. However, they are also commonly used as inlet profiles with other turbulence models (e.g. [33, 34, 35, 87, 91]).

The inlet profiles for U, k and ε used for the simulations in the present study are those for neutral stratification of the atmospheric boundary layer [34, 84]. For the fairly low wind speed conditions in the present study, using profiles for unstable stratification could have been better. However, these profiles might suffer from horizontal inhomogeneity (e.g. [34]), and further work on consistent CFD simulation of stable and unstable atmospheric boundary layers is required. In addition, it should be noted that the area with explicitly modelled buildings (i.e. with their main shapes and dimensions) in the present study is larger than the area of interest (Bergpolder Zuid). This way, the incident profiles (i.e. those to which the area of interest is subjected) are partly developed by these surroundings buildings and the surrounding ground roughness.

Concerning the validation methodology, space-averaged values for temperature were used to show that CFD can be an effective tool for the reproduction of the daily temperature variations in an urban area. However, if the focus would be on a smaller scale (i.e. building or road surface, a small street), then other, more detailed validation data with a higher spatial resolution would have been needed. With the current settings of the simulations for wind flow and heat transfer, the present study has demonstrated the capability and potential of CFD for predicting urban surface temperatures.

Water vapor transfer inside urban regions can also affect the temperature field. Especially localized sources of evapotranspiration (vegetation or water facilities) can significantly affect temperature distribution around the regions where they are located. Note however that in Bergpolder, vegetation is very limited and water facilities are absent. In addition, the relative humidity in the air might be important for the latent heat transfer in an urban area. In this study, water vapor transfer is considered as a sink term of evapotranspiration, which is effective only during daytime (between 6:00 h and 18:00 h), and the value for the term is based on previous theoretical and observational studies. The evapotranspiration sink term can be based upon one of the models developed for energy balance models [20,22] or can be solved coupled to the flow and temperature equations, which would require additional computational cost.

7. Conclusion

Studies on urban microclimate are gaining importance given the possible negative effects of high temperatures in urban areas on human mortality and morbidity and building energy demand. So far, these studies have been based on observational approaches (e.g. field measurements) and simulation approaches about urban microclimate have used mostly energy balance models. For the analysis of urban microclimate, the main weakness of energy balance models is that the velocity field is not directly modeled. On the other hand, in CFD, velocity field can be coupled with temperature field. Therefore CFD has the potential to be an important tool for the deterministic analysis of urban microclimate and consequently for the analysis of adaptation measures in building and urban scale.

This paper has presented unsteady CFD simulations considering wind flow and heat transfer (conduction, convection and radiation), investigating the Bergpolder Zuid region in Rotterdam, the Netherlands. The simulations were performed using the 3D URANS approach with the realizable k-ε turbulence model on a high-resolution grid. Most of the factors affecting the urban microclimate (shortwave, longwave radiation, wind velocity, evapotranspiration, and heat storage) were considered within the simulations whereas only the effect of anthropogenic heat sources was omitted.

In order to validate the simulation results of surface temperatures inside the urban area, data obtained from satellite images is used. The images were collected during the July 2006 heat wave and the results were reported by Klok et al. [79]. Meteorological conditions of the days corresponding to the data from satellite images were acquired from the KNMI database. Hourly data obtained from the KNMI included wind speed, wind direction, air temperature and solar radiation. Simulations are performed with respect to the meteorological data of 15 until 19 July 2006. Simulation results and reported data were compared and showed fairly good accuracy with the simulation results having only an average 7.9% difference with the experimental data (minimum deviation is 0.3% and the maximum deviation is 24.2%). The presented CFD approach allows analyzing the effect of the heat storage mechanism and the wind-velocity pattern on the temperature field.

It is concluded that CFD has the potential of accurately predicting urban microclimate. Results from CFD simulations can therefore be used to identify problem areas and to evaluate the effect of adaptation measures such as urban greening and evaporative cooling. Further work will therefore focus on the application of the CFD URANS approach for the evaluation of climate change adaptation measures.

Acknowledgements

This research was supported by the Dutch Knowledge for Climate Research Program within the theme Climate Proof Cities (CPC).

References

[1] Haines A, Kovats RS, Campbell-Lendrum D, Corvalan C. Climate change and human health: impacts, vulnerability and public health. Public Health 2006;120:585–96.
[2] Watkiss P. The ClimateCOST Project, Final Report, Volume 1: Europe. Stock Environ Inst 2011.
[3] Xu P, Huang YJ, Miller N, Schlegel N, Shen P. Impacts of climate change on building heating and cooling energy patterns in California. Energy 2012;44:792–804.
[4] Changnon SA, Kunkel EK, Reinke BC. Impacts and responses to the 1995 heat wave: A call to action. Bull Am Meteorol Soc 1996;77:1497–506.
[5] Van Garssen J, Harmsen C, de Beer J. Effect of the summer 2003 heat wave on mortality in the Netherlands. Eurosurveillance 2005;10:165–7.
[6] Conti S, Meli P, Minelli G, Solimini R, Toccaceli V, Vichi M, et al. Epidemiologic study of mortality during the Summer 2003 heat wave in Italy. Environ Res 2005;98:390–9.
[7] Sarrat C, Lemonsu a, Masson V, Guedalia D. Impact of urban heat island on regional atmospheric pollution. Atmos Environ 2006;40:1743–58.
[8] Tan J, Zheng Y, Tang X, Guo C, Li L, Song G, et al. The urban heat island and its impact on heat waves and human health in Shanghai. Int J Biometeorol 2010;54:75–84.
[9] Memon RA, Leung DYC, Liu C-H, Leung MKH. Urban heat island and its effect on the cooling and heating demands in urban and suburban areas of Hong Kong. Theor Appl Climatol 2010;103:441–50.
[10] Emmanuel R, Krüger EL. Urban heat island and its impact on climate change resilience in a shrinking city: The case of Glasgow, UK. Build Environ 2012;53:137–49.
[11] Kolokotroni M, Ren X, Davies M, Mavrogianni A. London's urban heat island: Impact on current and future energy consumption in office buildings. Energy Build 2012;47:302–11.
[12] Angel S, Sheppard SC, Civco DL. The dynamics of global urban expansion. Washington DC: 2005.
[13] United Nations. World Urbanization Prospects: The 2011 Revision. New York: 2012.
[14] Smith C, Levermore G. Designing urban spaces and buildings to improve sustainability and quality of life in a warmer world. Energy Policy 2008;36:4558–62.
[15] Mills G. Progress toward sustainable settlements: a role for urban climatology. Theor Appl Climatol 2005;84:69–76.
[16] Moonen P, Defraeye T, Dorer V, Blocken B, Carmeliet J. Urban Physics: Effect of the micro-climate on comfort, health and energy demand. Front Archit Res 2012;1:197–228.
[17] Arnfield J. Two decades of urban climate research: A review of turbulence, exchanges of energy and water, and the urban heat island. Int J Climatol 2003;23:1–26.
[18] Mirzaei PA, Haghighat F. Approaches to study Urban Heat Island – Abilities and limitations. Build Environ 2010;45:2192–201.
[19] Oke TR. The energetic basis of the urban heat island. Q J R Meteorol Soc 1982;108:1–24.
[20] Grimmond C, Oke T. An evapotranspiration-interception model for urban areas. Water Resour Res 1991;27:1739–55.
[21] Arnfield J, Grimmond CSB. An urban canyon energy budget model and its application to urban storage heat flux modeling. Energy Build 1998;27:61–8.
[22] Masson V. A physically-based scheme for the urban energy budget in atmospheric models. Boundary-Layer Meteorol 2000;94:357–97.
[23] Martilli A, Clappier A, Rotach M. An urban surface exchange parameterisation for mesoscale models. Boundary-Layer Meteorol 2002;104:261–304.
[24] Nunez M, Oke TR. Modeling the daytime urban surface energy balance. Geogr Anal 1980;12:373–86.
[25] Oke TR, Zeuner G, Jauregui E. The surface energy balance in Mexico City. Atmos Environ Part B Urban Atmos 1992;26:433–44.
[26] Christen A, Vogt R. Energy and radiation balance of a central European city. Int J Climatol 2004;24:1395–421.
[27] Offerle B, Grimmond CSB, Fortuniak K, Kłysik K, Oke TR. Temporal variations in heat fluxes over a central European city centre. Theor Appl Climatol 2005;84:103–15.
[28] Oke TR. Boundary Layer Climates. 2nd ed. London: Methuen; 1987.
[29] Erell E, Pearlmutter D, Williamson T. Urban Microclimate: Designing the Spaces Between Buildings. 1st ed. London: Earthscan; 2011.

[30] Blocken B. 50 years of Computational Wind Engineering: Past, Present and Future. J Wind Eng Ind Aerodyn 2014;In press.
[31] Casey M, Wintergerste T. ERCOFTAC Special Interest Group on “Quality and Trust in Industrial CFD” - Best Practice Guidelines. 2000.
[32] Jakeman AJ, Letcher RA, Norton JP. Ten iterative steps in development and evaluation of environmental models. Environ Model Softw 2006;21:602–14.
[33] Franke J, Hellsten A, Schlünzen H, Carissimo B. Best practice guideline for the CFD simulation of flows in the urban environment. Hamburg: 2007.
[34] Blocken B, Stathopoulos T, Carmeliet J. CFD simulation of the atmospheric boundary layer: wall function problems. Atmos Environ 2007;41:238–52.
[35] Tominaga Y, Mochida A, Yoshie R, Kataoka H, Nozu T, Yoshikawa M, et al. AIJ guidelines for practical applications of CFD to pedestrian wind environment around buildings. J Wind Eng Ind Aerodyn 2008;96:1749–61.
[36] Van Hooff T, Blocken B. Coupled urban wind flow and indoor natural ventilation modelling on a high-resolution grid: A case study for the Amsterdam ArenA stadium. Environ Model Softw 2010;25:51–65.
[37] Mochida A, Lun IYF. Prediction of wind environment and thermal comfort at pedestrian level in urban area. J Wind Eng Ind Aerodyn 2008;96:1498–527.
[38] Blocken B, Stathopoulos T, Carmeliet J, Hensen J. Application of CFD in building performance simulation for the outdoor environment: an overview. J Build Perform Simul 2011;4:157–84.
[39] Murakami S, Ooka R, Mochida A, Yoshida S. CFD analysis of wind climate from human scale to urban scale. J Wind Eng Ind Aerodyn 1999;81:57–81.
[40] Stathopoulos T. Pedestrian level winds and outdoor human comfort. J Wind Eng Ind Aerodyn 2006;94:769–80.
[41] Yoshie R, Mochida A, Tominaga Y, Kataoka H, Harimoto K, Nozu T, et al. Cooperative project for CFD prediction of pedestrian wind environment in the Architectural Institute of Japan. J Wind Eng Ind Aerodyn 2007;95:1551–78.
[42] Blocken B, Janssen WD, van Hooff T. CFD simulation for pedestrian wind comfort and wind safety in urban areas: General decision framework and case study for the Eindhoven University campus. Environ Model Softw 2012;30:15–34.
[43] Blocken B, Stathopoulos T, Saathoff P, Wang X. Numerical evaluation of pollutant dispersion in the built environment: Comparisons between models and experiments. J Wind Eng Ind Aerodyn 2008;96:1817–31.
[44] Gousseau P, Blocken B, Stathopoulos T, van Heijst GJF. CFD simulation of near-field pollutant dispersion on a high-resolution grid: A case study by LES and RANS for a building group in downtown Montreal. Atmos Environ 2011;45:428–38.
[45] Tominaga Y, Stathopoulos T. CFD simulation of near-field pollutant dispersion in the urban environment: A review of current modeling techniques. Atmos Environ 2013;79:716–30.
[46] Vos PEJ, Maiheu B, Vankerkom J, Janssen S. Improving local air quality in cities: to tree or not to tree? Environ Pollut 2013;183:113–22.
[47] Di Sabatino S, Buccolieri R, Salizzoni P. Recent advancements in numerical modelling of flow and dispersion in urban areas: A short review. Int J Environ Pollut 2013;52:172–91.
[48] Choi EC. Simulation of wind-driven-rain around a building. J Wind Eng Ind Aerodyn 1993;46:721–9.
[49] Blocken B, Carmeliet J. A review of wind-driven rain research in building science. J Wind Eng Ind Aerodyn 2004;92:1079–130.
[50] Kato S, Murakami S, Mochida A, Akabayashi S, Tominaga Y. Velocity-pressure field of cross ventilation with open windows analyzed by wind tunnel and numerical simulation. J Wind Eng Ind Aerodyn 1992;44:2575–86.
[51] Chen Q. Ventilation performance prediction for buildings: A method overview and recent applications. Build Environ 2009;44:848–58.
[52] Ramponi R, Blocken B. CFD simulation of cross-ventilation for a generic isolated building: Impact of computational parameters. Build Environ 2012;53:34–48.
[53] Bjerg B, Cascone G, Lee I-B, Bartzanas T, Norton T, Hong S-W, et al. Modelling of ammonia emissions from naturally ventilated livestock buildings. Part 3: CFD modelling. Biosyst Eng 2013;116:259–75.
[54] Mochida A, Murakami S, Ojima T, Kim S, Ooka R, Sugiyama H. CFD analysis of mesoscale climate in the Greater Tokyo area. J Wind Eng Ind Aerodyn 1997;67 & 68:459–77.
[55] Bruse M, Fleer H. Simulating surface–plant–air interactions inside urban environments with a three dimensional numerical model. Environ Model Softw 1998;13:373–84.

[56] Ashie Y, Ca VT, Asaeda T. Building canopy model for the analysis of urban climate. J Wind Eng Ind Aerodyn 1999;81:237–48.
[57] Ca VT, Asaeda T, Ashie Y. Development of a numerical model for the evaluation of the urban thermal environment. J Wind Eng Ind Aerodyn 1999;81:181–96.
[58] Fujino T, Asaeda T, Thanh Ca V. Numerical analyses of urban thermal environment in a basin climate – application of a k–ε model to complex terrain. J Wind Eng Ind Aerodyn 1999;81:159–69.
[59] Takahashi K, Yoshida H, Tanaka Y, Aotake N, Wang F. Measurement of thermal environment in Kyoto city and its prediction by CFD simulation. Energy Build 2004;36:771–9.
[60] Chen H, Ooka R, Harayama K, Kato S, Li X. Study on outdoor thermal environment of apartment block in Shenzhen, China with coupled simulation of convection, radiation and conduction. Energy Build 2004;36:1247–58.
[61] Li X, Yu Z, Zhao B, Li Y. Numerical analysis of outdoor thermal environment around buildings. Build Environ 2005;40:853–66.
[62] Murakami S. Environmental design of outdoor climate based on CFD. Fluid Dyn Res 2006;38:108–26.
[63] Priyadarsini R, Hien WN, Wai David CK. Microclimatic modeling of the urban thermal environment of Singapore to mitigate urban heat island. Sol Energy 2008;82:727–45.
[64] Chen H, Ooka R, Kato S. Study on optimum design method for pleasant outdoor thermal environment using genetic algorithms (GA) and coupled simulation of convection, radiation and conduction. Build Environ 2008;43:18–30.
[65] Lin B, Li X, Zhu Y, Qin Y. Numerical simulation studies of the different vegetation patterns' effects on outdoor pedestrian thermal comfort. J Wind Eng Ind Aerodyn 2008;96:1707–18.
[66] Dimitrova R, Sini J-F, Richards K, Schatzmann M, Weeks M, Perez García E, et al. Influence of Thermal Effects on the Wind Field Within the Urban Environment. Boundary-Layer Meteorol 2009;131:223–43.
[67] Chen H, Ooka R, Huang H, Tsuchiya T. Study on mitigation measures for outdoor thermal environment on present urban blocks in Tokyo using coupled simulation. Build Environ 2009;44:2290–9.
[68] Hsieh C-M, Chen H, Ooka R, Yoon J, Kato S, Miisho K. Simulation analysis of site design and layout planning to mitigate thermal environment of riverside residential development. Build Simul 2010;3:51–61.
[69] Memon RA, Leung DYC, Liu C-H. Effects of building aspect ratio and wind speed on air temperatures in urban-like street canyons. Build Environ 2010;45:176–88.
[70] Memon RA, Leung DYC. On the heating environment in street canyon. Environ Fluid Mech 2010;11:465–80.
[71] Kaoru I, Akira K, Akikazu K. The 24-h unsteady analysis of air flow and temperature in a real city by high-speed radiation calculation method. Build Environ 2011;46:1632–8.
[72] Berkovic S, Yezioro A, Bitan A. Study of thermal comfort in courtyards in a hot arid climate. Sol Energy 2012;86:1173–86.
[73] Ma J, Li X, Zhu Y. A simplified method to predict the outdoor thermal environment in residential district. Build Simul 2012;5:157–67.
[74] Bo-ot LM, Wang Y-H, Chiang C-M, Lai C-M. Effects of a Green Space Layout on the Outdoor Thermal Environment at the Neighborhood Level. Energies 2012;5:3723–35.
[75] Qu Y, Milliez M, Musson-Genon L, Carissimo B. Numerical study of the thermal effects of buildings on low-speed airflow taking into account 3D atmospheric radiation in urban canopy. J Wind Eng Ind Aerodyn 2012;104-106:474–83.
[76] Yang X, Zhao L, Bruse M, Meng Q. Evaluation of a microclimate model for predicting the thermal behavior of different ground surfaces. Build Environ 2013;60:93–104.
[77] Allegrini J, Dorer V, Carmeliet J. Buoyant flows in street canyons: Validation of CFD simulations with wind tunnel measurements. Build Environ 2014;72:63–74.
[78] Shih T-H, Liou WW, Shabbir A, Yang Z, Zhu J. A new k-ϵ eddy viscosity model for high reynolds number turbulent flows. Comput Fluids 1995;24:227–38.
[79] Klok L, Zwart S, Verhagen H, Mauri E. The surface heat island of Rotterdam and its relationship with urban surface characteristics. Resour Conserv Recycl 2012;64:23–9.
[80] Parry ML, Canziani OF, Palutikof JP, van der Linden PJ, Hanson CE. Contribution of Working Group II to the Fourth Assessment Report of the Intergovernmental Panel on Climate Change, 2007. Cambridge: 2007.
[81] Albers RAW, Blocken B, Bosch PR. Overview of challenges and achievements in the Climate Proof Cities program. Build Environ 2014;This issue.
[82] Heusinkveld BG, Steeneveld GJ, van Hove LWA, Jacobs CMJ, Holtslag AAM. Spatial variability of the Rotterdam urban heat island as influenced by urban land use. J Geophys Res Atmos 2013.

[83] Wieringa J. Updating the Davenport roughness classification. J Wind Eng Ind Aerodyn 1992;44:357–68.
[84] Richards P, Hoxey R. Appropriate boundary conditions for computational wind engineering models using the k-ε turbulence model. J Wind Eng Ind Aerodyn 1993;46 & 47:145–53.
[85] Launder BE, Spalding DB. The numerical computation of turbulent flows. Comput Methods Appl Mech Eng 1974;3:269–89.
[86] Cebeci T, Bradshaw P. Momentum Transfer in Boundary Layers. New York: Hemisphere Publishing Corporation; 1977.
[87] Blocken B, Defraeye T, Derome D, Carmeliet J. High-resolution CFD simulations for forced convective heat transfer coefficients at the facade of a low-rise building. Build Environ 2009;44:2396–412.
[88] Murakami S. Comparison of various turbulence models applied to a bluff body. J Wind Eng Ind Aerodyn 1993;46:21–36.
[89] Grimmond C, Oke T. Turbulent heat fluxes in urban areas: observations and a local-scale urban meteorological parameterization scheme (LUMPS). J Appl Meteorol 2002:792–810.
[90] ANSYS Inc. ANSYS FLUENT 12.0 Theory Guide 2009.
[91] Allegrini J, Dorer V, Carmeliet J. Analysis of convective heat transfer at building façades in street canyons and its influence on the predictions of space cooling demand in buildings. J Wind Eng Ind Aerodyn 2012;104-106:464–73.

Table 1: Overview of CFD studies on thermal environment in urban areas. The entry "Causes considered" refers to the list of possible UHI causes by Oke [20,29], which are (1) amplified short-wave radiation gain; (2) amplified long-wave radiation gain from the sky; (3) decreased long-wave radiation loss; (4) anthropogenic heat sources; (5) increased heat storage; (6) less evapotranspiration and (7) decreased turbulent heat transport.

Authors (year)	Ref.	Scale	Configuration	Causes considered	Steady vs. unsteady	Validation
Mochida et al. (1997)	[54]	Mesoscale (3D)	No buildings	1, 2, 3, 4, 5, 6	Unsteady	Yes
Bruse and Fleer (1998)	[55]	Microscale (3D)	3D generic urban	1, 3, 5, 6, 7	Unsteady	No
Ashie et al. (1999)	[56]	Microscale (2D)	2D street canyon	1, 4, 6, 7	Unsteady	No
Ca et al. (1999)	[57]	Microscale (2D)	2D buildings	1, 3, 4, 6	Unsteady	Yes
Fujino et al. (1999)	[58]	Mesoscale (3D)	No buildings	1, 2, 5, 6	Unsteady	Yes
Takahashi el al. (2004)	[59]	Microscale (3D)	3D applied urban	1, 2, 3, 6, 7	Unsteady	Yes
Chen et al. (2004)	[60]	Microscale (3D)	3D applied urban	1, 3, 4, 6 , 7	Unsteady	Yes
Li et al. (2005)	[61]	Microscale (3D)	Single building	1, 2, 3, 5	Quasi-steady	Yes
Murakami (2006)	[62]	Microscale (3D)	3D generic urban	1, 3, 4, 6, 7	Unsteady	No
Priyadarsini et al. (2008)	[63]	Microscale (3D)	3D applied urban	1, 4, 5, 7	Unsteady	Yes
Chen et al. (2008)	[64]	Microscale (3D)	3D generic urban	1, 3, 7	Unsteady	No
Lin et al. (2008)	[65]	Microscale (3D)	3D generic urban	1, 2, 5, 6, 7	Unsteady	No
Dimitrova et al. (2009)	[66]	Microscale (3D)	3D generic urban	1, 2, 7	Steady	Yes
Chen et al. (2009)	[67]	Microscale (3D)	3D applied urban	1, 3, 4, 5, 6, 7	Unsteady	No
Hsieh et al. (2010)	[68]	Microscale (3D)	3D applied urban	1, 2, 5, 6, 7	Unsteady	No
Memon et al. (201)	[69]	Microscale (2D)	2D street canyon	1, 7	Steady	Yes
Memon and Leung (2010)	[70]	Microscale (2D)	2D street canyon	7	Steady	Yes
Kaoru et al. (2011)	[71]	Microscale (3D)	3D applied urban	1, 2, 3, 5, 7	Unsteady	No
Berkovic et al (2012)	[72]	Microscale (3D)	3D generic courtyard	1, 2, 3, 5, 6, 7	Unsteady	Yes
Ma et al. (2012)	[73]	Microscale (3D)	3D applied urban	1, 2, 5, 6, 7	Unsteady	Yes
Bo-ot et al. (2012)	[74]	Microscale (3D)	3D generic urban	3, 4, 7	Unsteady	No
Qu et al. (2012)	[75]	Microscale (3D)	3D generic urban	1, 2, 3, 5, 7	Unsteady	No
Yang et al. (2013)	[76]	Microscale (3D)	3D applied urban	1, 2, 3, 5, 6, 7	Unsteady	Yes
Allegrini et al. (2014)	[77]	Microscale (2D)	2D street canyon	7	Steady	Yes
Present study	[-]	Microscale (3D)	3D applied urban	1, 2, 3, 5, 6, 7	Unsteady	Yes

Table 2: Specifications of the materials used in this study.

Material	Density (kg/m^3)	Specific heat (J/kgK)	Thermal conductivity (W/mK)	Absorptivity	Emissivity
Earth	1150	650	1.5	0.6	0.90
Brick	1400	900	1.7	0.75	0.88

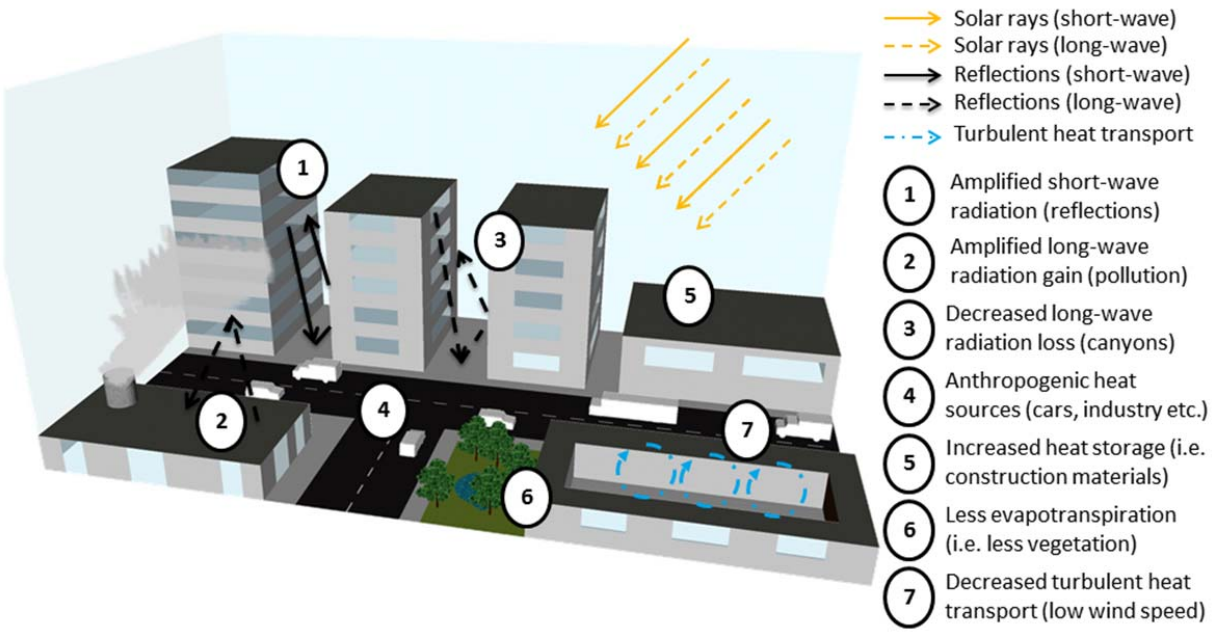

Figure 1: Representation of the possible causes of the UHI effect.

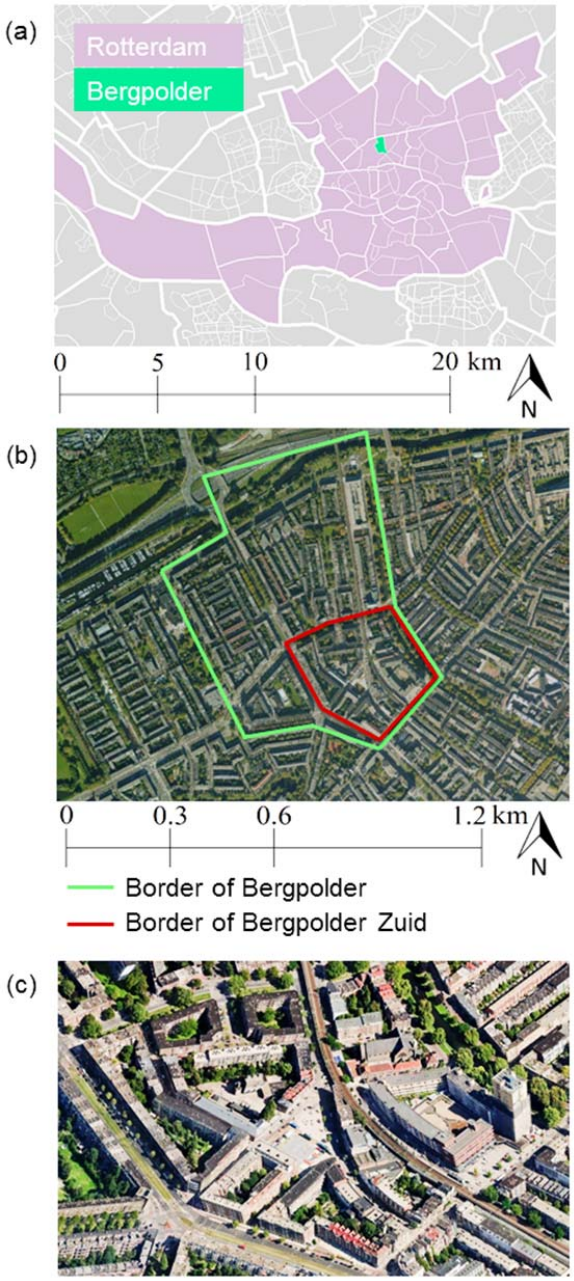

Figure 2: (a) Location of Bergpolder inside the city of Rotterdam (modified from Wikipedia[3]). (b) Top view with the borders of Bergpolder and Bergpolder Zuid (modified from Google Maps[2]). (c) Aerial view of Bergpolder Zuid (view from south) (modified from Google Maps[4]).

[3] Wikipedia source: http://commons.wikimedia.org/wiki/File:Rotterdamse_wijken-bergpolder.PNG
[4] Google maps source: http://goo.gl/maps/zEziy

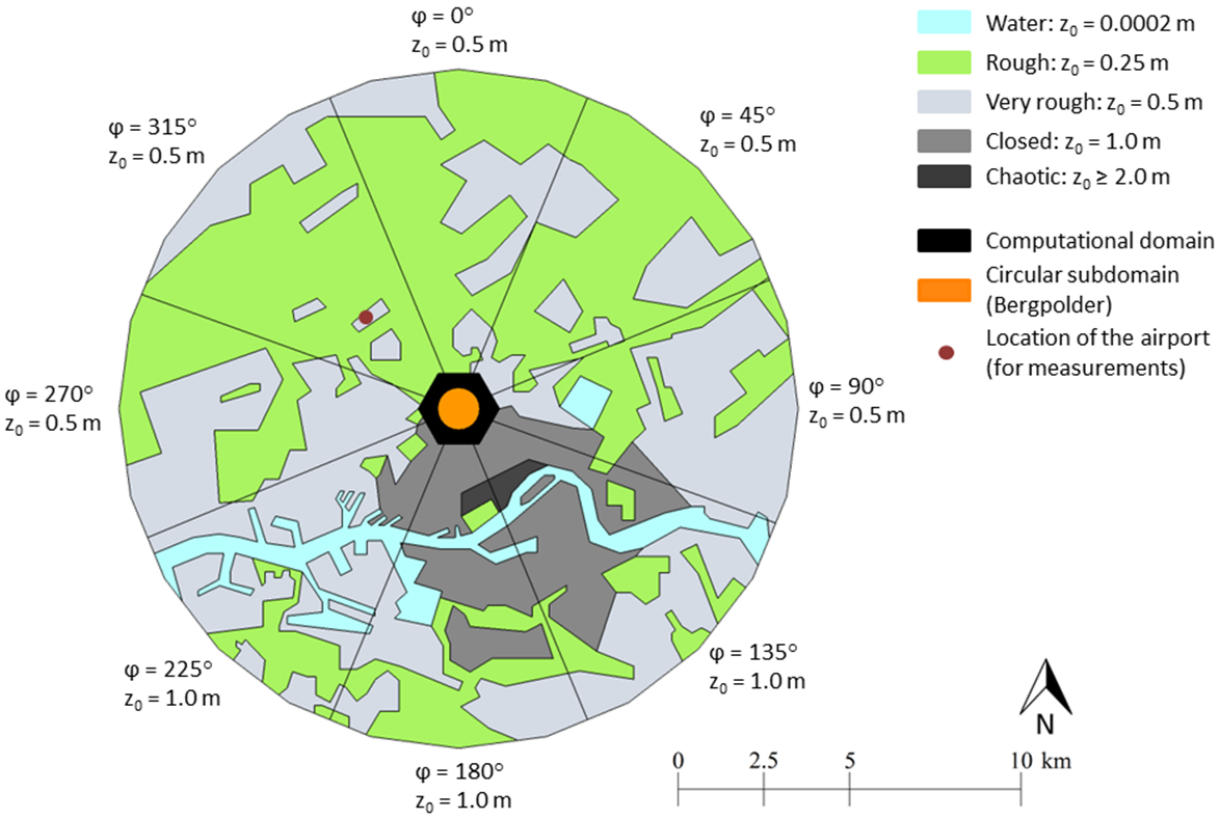

Figure 3: Terrain surrounding the modeled urban area with a radius of 10 km. The estimated aerodynamic roughness length (z_0) is shown for different angles. The computational domain used in this study is represented by the black hexagon in the middle.

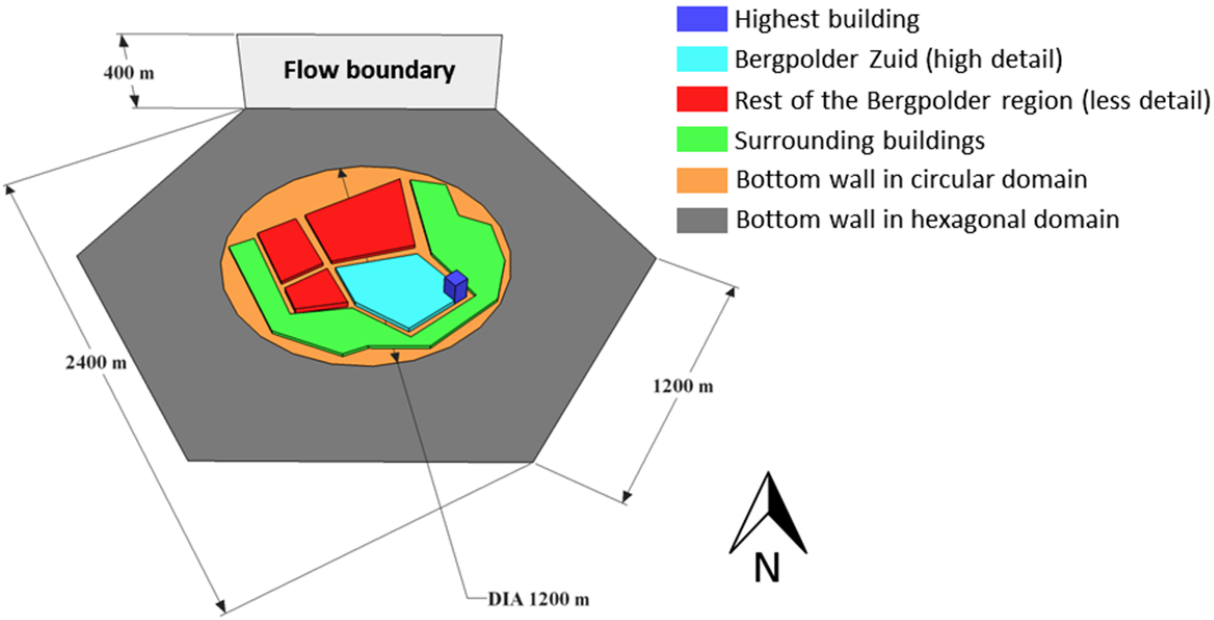

Figure 4: Computational domain. Different colors represent different categories of buildings in terms of detail in modeling.

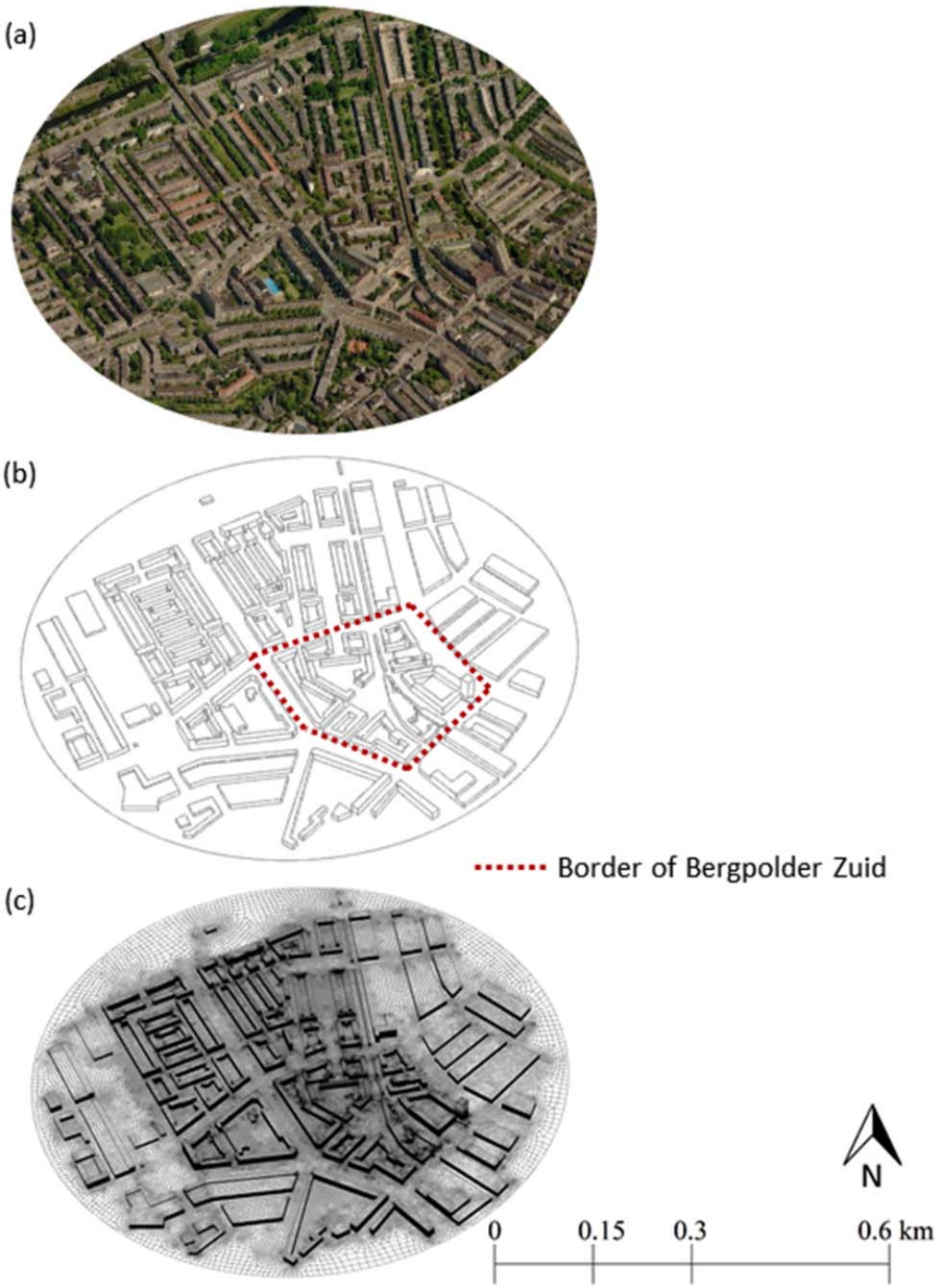

Figure 5: a) Aerial view of the Bergpolder region from south (source: Bing Maps[5]); b) Corresponding computational geometry; c) Computational grid on the building surfaces and on part of the ground surface. The intensity of black lines indicates areas with a higher mesh resolution (6,610,456 cells).

[5] Bing maps source: http://binged.it/17VliGv

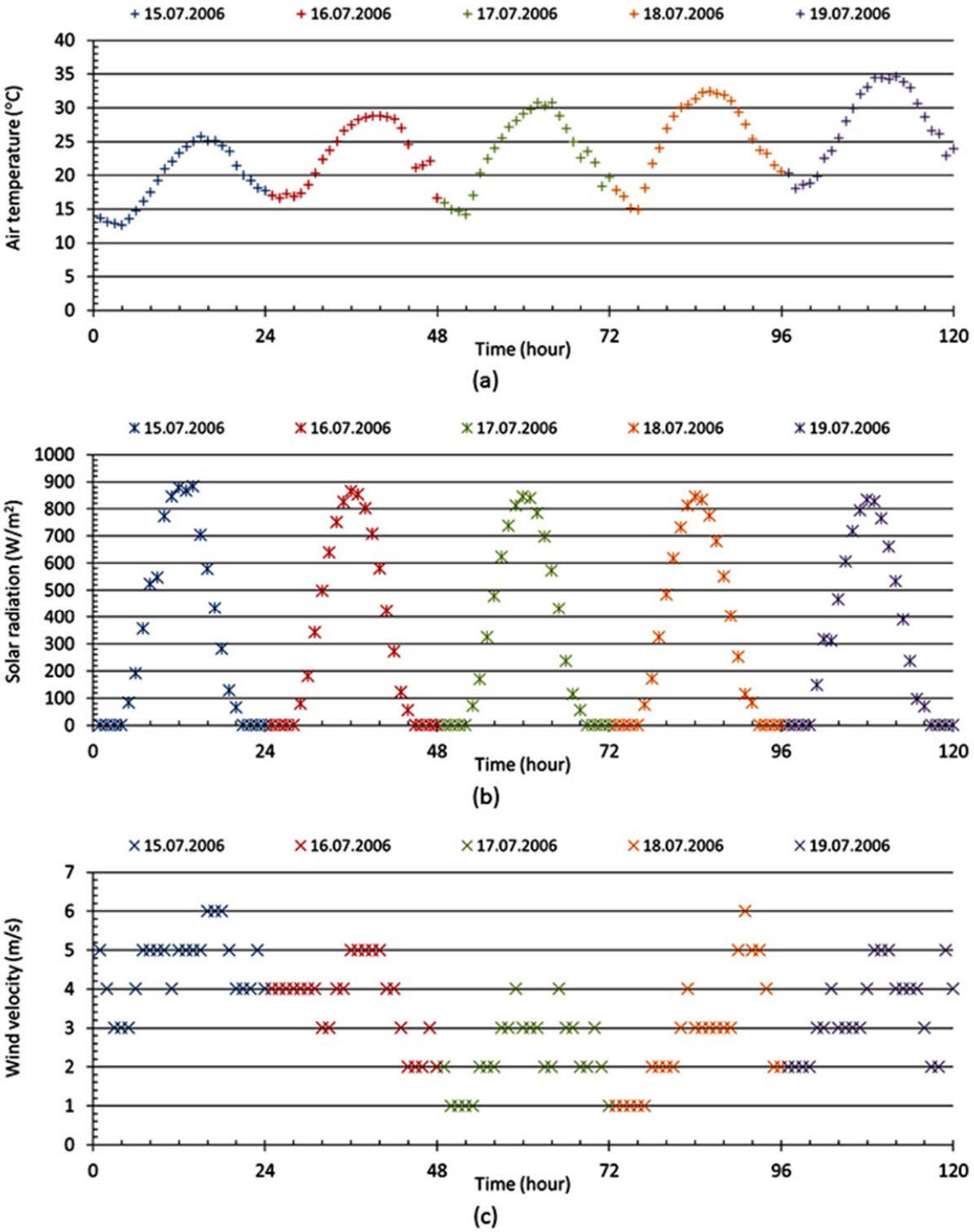

Figure 6: Meteorological data of Rotterdam (based on KNMI-Rotterdam weather station) during 15, 16, 17, 18 and 19 July 2006. Acquired from the hourly dataset of KNMI for: a) air temperature; b) solar radiation; c) wind velocity.

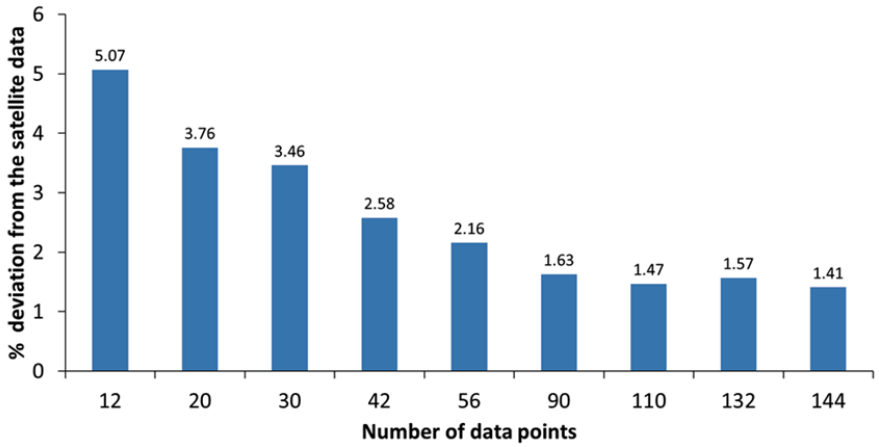

Figure 7: Results of the sensitivity analysis. Percentage deviation is calculated based on the satellite imagery data recorded at 12:10 h on July 15, 2006 and on CFD simulations for the same moment in time.

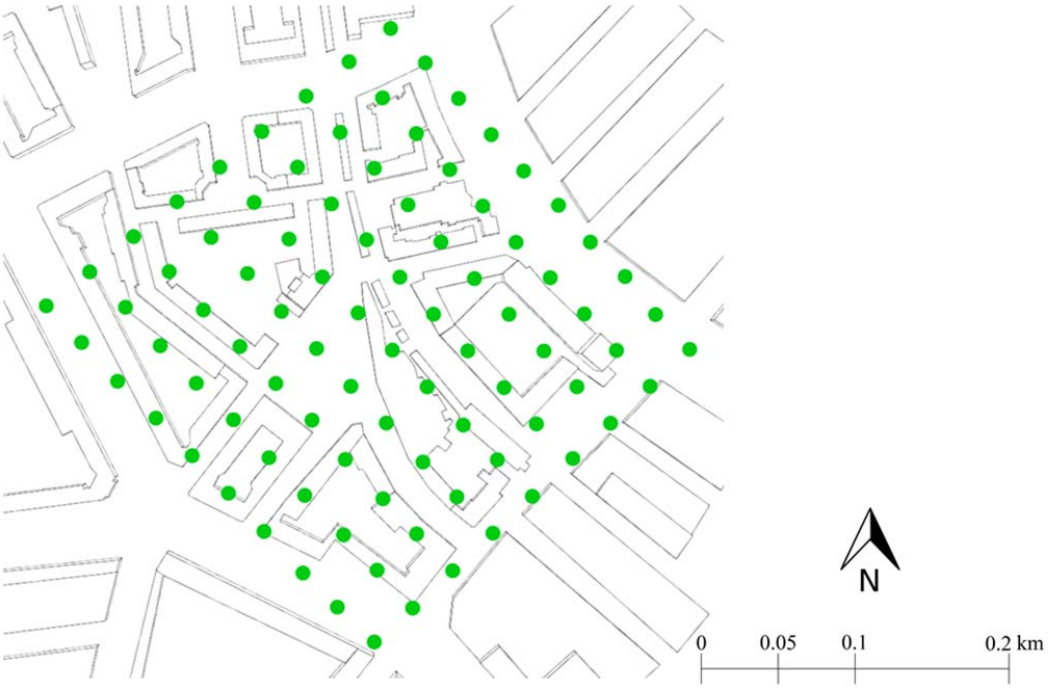

Figure 8: Location of sampling points on the building and street surfaces of Bergpolder Zuid. In total 90 (10 x 9) data points are placed equidistantly.

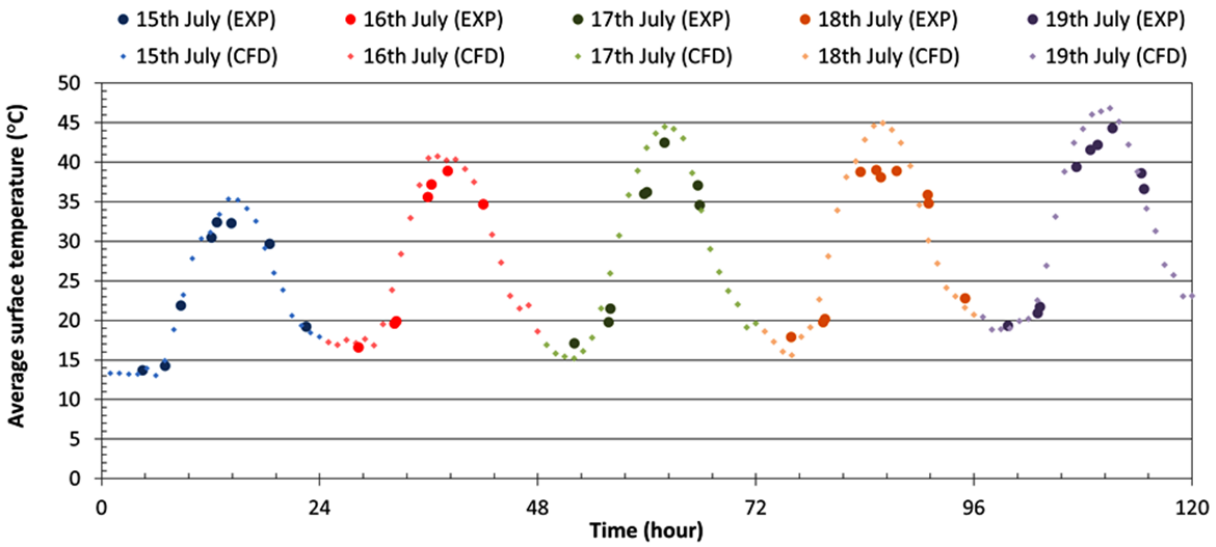

Figure 9: Comparison of CFD simulation results and data from satellite images of average surface temperatures for five consecutive days.

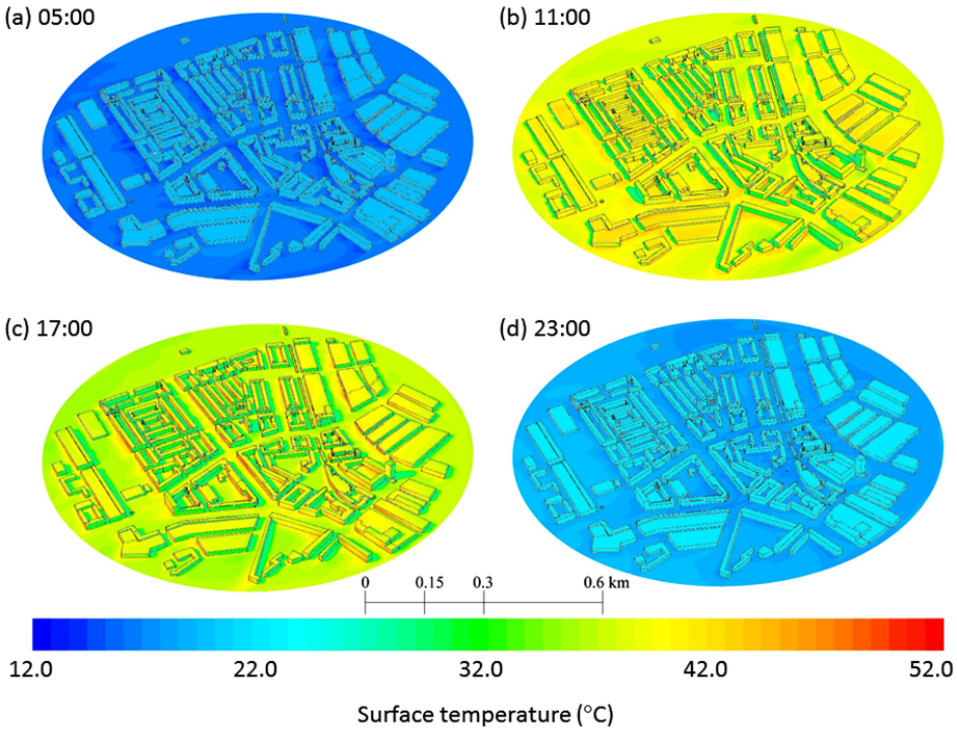

Figure 10: Contours of simulated temperatures for the Bergpolder region during 16 July 2006 at: a) 5:00 h; b) 11:00 h; c) 17:00 h; d) 23:00 h (view from south).

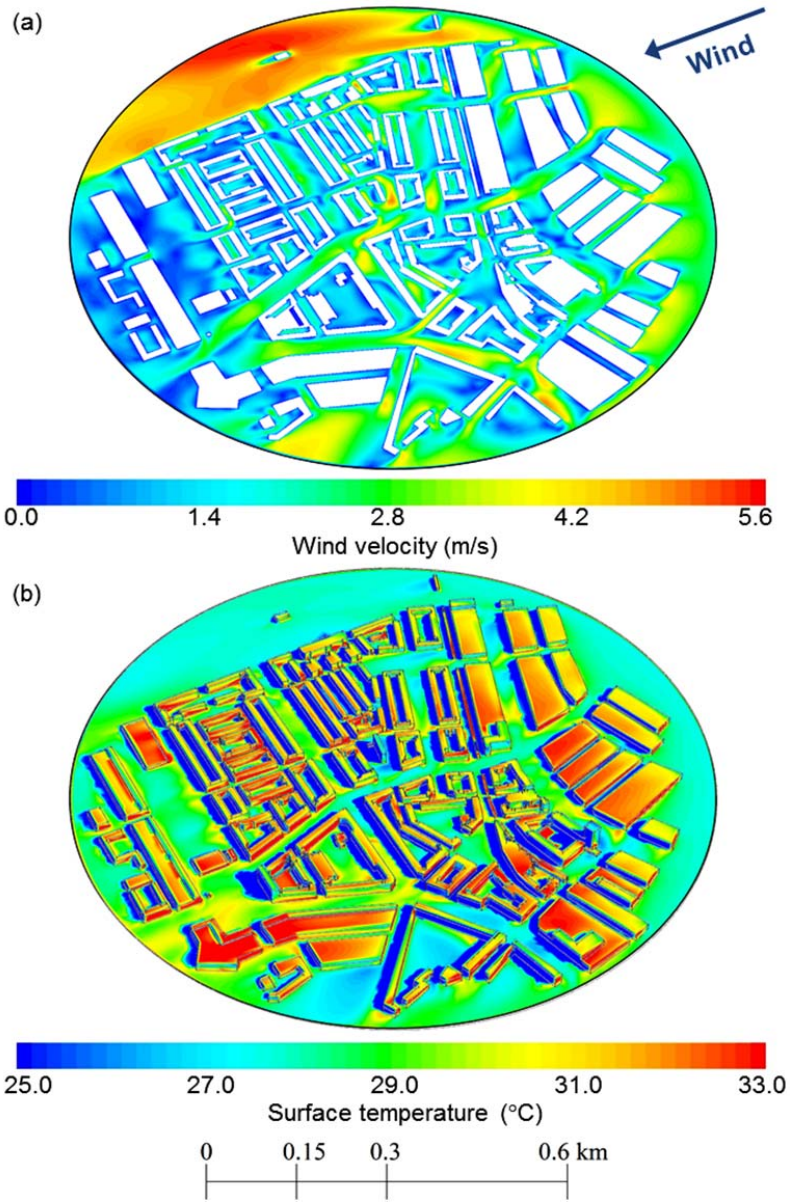

Figure 11: Simulation results for: a) wind velocity (m/s) at 1 meter height; and b) surface temperature (°C) for July 15 2006, 10:00 h. Both views are from south.